CrossMark

High-energy picosecond kHz optical parametric oscillator/amplifier tunable between 3 and 3.5 μm

D. Chuchumishev[1] · A. Trifonov[2] · B. Oreshkov[1] · X. Xu[3] · I. Buchvarov[1,4]

Abstract

We present a mid-IR tunable high-energy kHz optical parametric oscillator/amplifier (OPO/OPA) based on periodically poled stoichiometric lithium tantalate (PPSLT) nonlinear crystals. These two frequency conversion stages are pumped by a 1-μm-Nd-based master oscillator power amplifier (MOPA) system generating 800 ps pulses at 0.5 kHz with energy scalable up to ~ 40 mJ. The OPO/OPA stages are temperature tunable between 3 and 3.5 μm and provide pulses with energy 4.1 mJ and pulse duration of 600 ps.

1 Introduction

Soon after the development of the first lasers, researchers realized they possess tremendous potential as a precise surgical instrument due to their ability to confine energy into a small area and generate wavelengths that are either strongly or selectively absorbed in the target tissue. The ultimate goal of laser surgery applications has become the ablation of a defined volume of tissue while leaving the adjacent tissue biologically viable [1–5].

Since the optical absorption properties of tissues are governed by the electronic, vibrational, and rotational structures of the constituent biomolecules (proteins, melanin, hemoglobin and water) the widespread spectroscopic transitions of these tissue chromophores enable optical excitations in various spectral regions from the UV to the IR range. Due to the absence of mutagenic risks associated with the use

of UV lasers, IR lasers hold special promise for medical applications [6–9].

Initially the main source for medical applications such as tissue ablation and advanced neurosurgery with minimal collateral damage has been the mid-IR Free Electron Laser (FEL) [1, 10].Despite its great advantages providing high-pulse energy ($>>$ 1 mJ) and high-average power at mid-IR spectral range, the FEL system possesses serious drawbacks that are intrinsic to its underlying physical principles. Since FELs consist of a relativistic electron beam propagating through a periodic magnetic field, they are large-scale facilities whose operation requires highly qualified personal and substantial maintenance costs. These disadvantages prohibit the broad clinical usage of such facilities and present the need of a compact laser system that will generate tunable mid-IR radiation with high energy at high repetition rates.

A comprehensive review of the existing solid state mid-IR laser sources [11] shows that the main performance limitations of these devices are the output power and wavelength coverage. Typically, host materials for long-wavelength laser transitions are problematic for high-average power output and they rarely enable wavelength tunability. Thus, the most robust approach for generating mid-IR tunable radiation is through nonlinear optical down-conversion.

In recent years due to their exceptionally large nonlinearity and complete absence of spatial walk-off, periodically poled, quasi-phase-matched nonlinear materials are preferred for parametric conversion of radiation. Systems based on periodically poled lithium niobate (PPLN) have been presented, but they are either at high a repetition rate (10 kHz) and a very modest output energy (few

✉ I. Buchvarov
ivan.buchvarov@phys.uni-sofia.bg

1   Department of Physics, Sofia University, 5 James Bourchier Blvd., 1164 Sofia, Bulgaria

2   IBPhotonics Ltd, 19A Plovdivsko Pole St., 1756 Sofia, Bulgaria

3   Jiangsu Normal University, Xuzhou 221116, China

4   ITMO University, 197101 Saint Petersburg, Russia

micro-joules) [12] or at a low repetition rate (10 Hz) and a high output energy (3.4 mJ), but consequently very modest average output power [13]. Even though MgO doping of LN has increased its photorefractive damage threshold and decreased its originally very high coercive field, periodically poled stoichiometric lithium tantalate (PPSLT) has a lower coercive field (~ 2 kV/mm for PPLN and 0.8 kV/mm for PPSLT) and a higher photorefractive damage threshold, while being transparent in the mid-IR spectral range to 5 μm. Therefore, it has been suggested that PPSLT is a suitable candidate for more efficient devices, with either high-energy or high-average power output. This has been demonstrated for pump pulses with a few tens of nanosecond pulse duration at 30 Hz and 10 kHz repetition rate, respectively [14, 15]. Extreme results of 2-mJ pulses at 0.5 kHz and 270 ps pulse duration were already reported when using the PPSLT in OPO configuration [16].

In this work, we present a tabletop picosecond mid-IR system that is tunable near the water absorption peak at 3 μm. It consists of a OPO/OPA energy scalable frequency conversion stage pumped by a 1-μm-Nd-based MOPA generating up to 40 mJ pulses at 0.5 kHz repetition rate. The mid-IR output reaches 4.1 mJ pulse energy at 38 mJ pump and it is continuously tuned from 3 to 3.5 μm by PPSLT-temperature change from 265 to 40 °C. The obtained high-energy OPA output pulse duration is ~ 600 ps.

2 Experimental setup

2.1 Pump source at 1 μm

The pump source for the nonlinear conversion stage is based on the master oscillator power amplifier architecture designed for energy- and average-power scaling of single-mode, single-frequency Nd:YAG laser at 0.5–1 kHz repetition rate (Fig. 1). As a master oscillator, we use a passively Q-switched Nd:YAG micro-laser which is end-pumped by a fiber-coupled quasi-CW diode array. The pump pulse duration is 200 μs with peak power of 50W centered at 808 nm. The pump beam is delivered through an optical fiber with a 400 μm core and imaged in the active element through an aspheric lens objective with a 1:1 magnification. The single-longitudinal mode of operation is achieved with the utilization of a twisted-mode cavity [17] and the maximum energy of the polarized output is 300 μJ at 0.5 kHz with a pulse duration of 800 ps.

The output beam from the oscillator is collimated to 2 mm in diameter (at $1/e^2$ level) and is amplified by four passes through a side-pumped amplifier module which employs a 65 mm long, 0.6 at% doped Nd:YAG crystal. The crystal is 3 mm in diameter and is pumped in a three-fold geometry by three linear stacks, each one composed by six
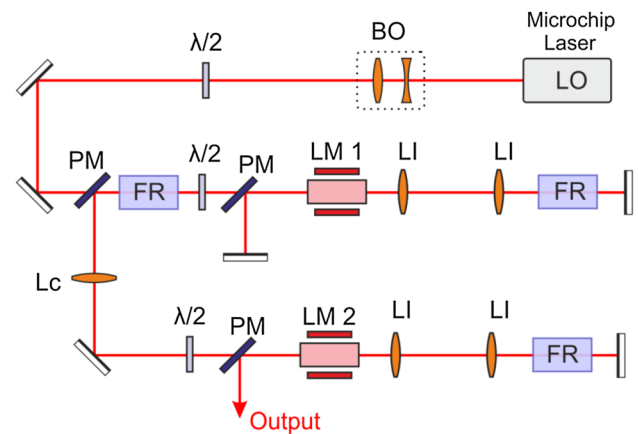

Fig. 1 Optical setup of the pump laser source at 1 micron. *LO* single transfer mode single-frequency microchip laser oscillator; *BO* beam transforming optics; *λ/2* half-wave plate; *PM* polarizing mirror; *LI* 4f-imaging lens; *LM1* side-pumped amplification module for 3-mm diameter active rod; *FR* π/4 Faraday rotator; *LC* collimated lens; *LM2* side-pumped amplification module for 5-mm diameter active rod

80-W QCW laser diode bars. The output beam from the first amplifier is collimated to 3.5 mm in diameter (at $1/e^2$ level) and is further amplified by two passes through a second amplifier module, which employs a Nd:YAG crystal (5 mm in diameter), pumped in a five-fold geometry by five linear stacks, each one with five 60-W QCW laser diode bars. The pump pulse duration in both amplifiers is 240 μs and a delay generator is used to synchronize the seed input time of the oscillator pulse for its maximum amplification.

In general, to achieve efficient energy extraction from a pulse amplifier, the energy density of the input signal must be close to the saturation density of the used laser material. Taken into account that the Nd:YAG media has a saturation density of 0.67 J/cm^2 and diameter of the first used rod is 3 mm, there is a need to reach the mJ energy level for the input pulses to extract efficiently the stored energy in the active media. Usually this is achieved through implementation of a preamplifier, but to minimize the technical complexity of the setup, a four-pass amplification scheme was used in the first amplification stage. Also, in both amplification stages a 4f-imaging system together with a Faraday rotator is employed to compensate for the thermally induced depolarization [18], occurring at high pump levels. The proposed 1-μm-laser architecture is suitable for energy- and average-power scaling and with its use, we have demonstrated up to 52 mJ single-mode and single-frequency operation at 0.75 kHz with 1.6-ns oscillator [19].

2.2 Frequency down-conversion to mid-IR

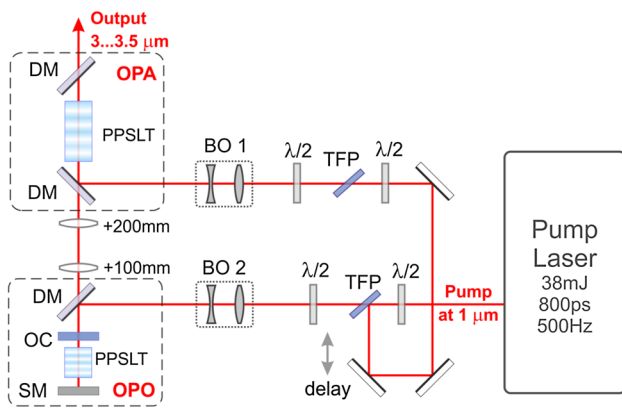Figure 2 shows the experimental layout of the frequency down-conversion of the 1-μm-Nd-based MOPA radiation

Fig. 2 Optical scheme of the frequency conversion stages: *TFP* thin-film polarizer; *λ/2* half-wave plate; *DM* dichroic mirror; *SM* silver mirror

and it is realized in two stages. In the first stage, an optical parametric oscillator (OPO) is used to convert the 1 μm radiation to mid-IR which is then amplified in the second stage through a single-pass optical parametric amplifier (OPA).

For the OPO, a singly resonant cavity was used with a two-pass pumping. The employed nonlinear crystal is a 20 mm long, 10 mm wide, and 3.2 mm (along z axis) thick PPSLT crystal (manufactured by Deltronic Crystal Industries Inc., NJ) with three polled zones with different domain inversion periods (30.2, 30.3 and 30.4 μm, respectively), equally spaced along the width of the crystal. The crystal is antireflection coated for the pump, the signal and idler waves and is pumped through the output coupler which transmits 99% of the pump, 98% of the idler wave and reflects 99.9% of the signal wave. The rear mirror is silver coated with reflection of more than 97% for the three interacting waves. To separate the pump and idler waves at the output of the OPO a dichroic mirror is used that transmits 97% of the idler and reflects 99% of the pump.

The idler output from the OPO is imaged in the OPA with two CaF_2 lenses with focal lengths of 100 and 200 mm. The OPA consist of an identical PPSLT crystal that is 37 mm

long. Both nonlinear crystals are mounted in ovens that can be heated up to 265 °C with a 0.1 °C accuracy and the OPO cavity length is confined by the oven design to 27 mm. The output of the developed 1-μm MOPA is divided in two by a thin-film polarizer (TFP) and half-wave plate so that one of the beams is used to pump the OPO and the other is used to pump the OPA. Before the OPA, a second set of TFP and half-wave plate is added to precisely control the pump energy of the OPA. Two lens objectives are used to form the desired pump beam size in the frequency conversion stages and the result is 1.9×2.0 mm (at $1/e^2$ level) and 2.7×2.8 mm for the OPO and OPA, respectively. The pump path from the MOPA to the OPA is about 35 cm longer than the path to the OPO to compensate for the build-up time of the OPO and optimize the relative timing of the pulses input to the OPA. Dichroic mirrors at 45° that are highly reflective for the pump and highly transmitting for the idler are used to couple the idler seed and the pump into the OPA (see Fig. 2).

3 Results and discussion

When seeded with the maximum microchip oscillator output of 300 μJ, the pulse energy of the amplifier at 1 μm reaches 18 mJ after four passes through the first amplification module and 38 mJ after further two passes through the second amplification module (see Fig. 3a). Using low-doped Nd:YAG rods in the two amplifiers, a uniform gain is achieved and the thermal effects are kept low so that beam quality deterioration is minimal. The M^2 factor is measured with a silicon CCD camera and a lens with focal length of 150 mm and the estimated values are 1.05×1.02 for the oscillator and 1.5×1.2 for the output of the MOPA (Fig. 3b). To measure the duration of the laser pulses, a fast InGaAs photodiode and a 4-GHz oscilloscope were used. The estimated value of the 1-μm-MOPA pulse duration is 800 ps after deconvolution with the response time of the measuring system (160 ps).

As mentioned before, the output of the MOPA is divided into two beams: one is used to pump the OPO and the other

Fig. 3 **a** Amplifier output energy versus input seed energy: after passing through the first amplification stage (blue dots); after two additional passes through the second amplification stage (red rectangles); **b** beam radius measurements near the waist and a few relay ranges
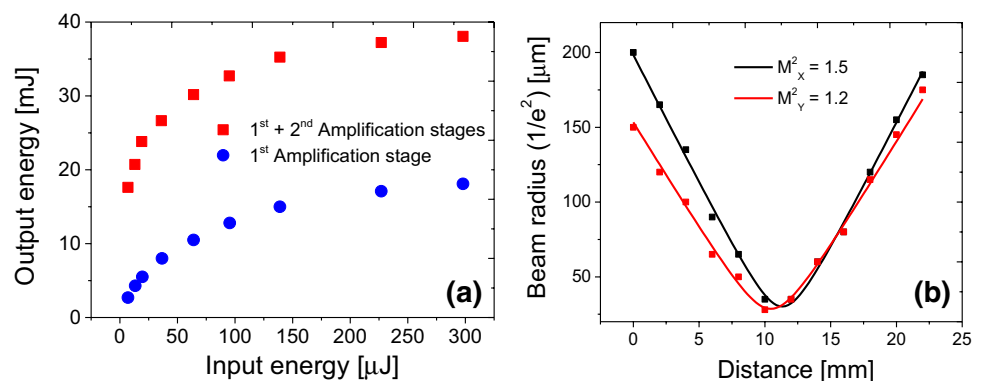
to pump the OPA. The measured OPO threshold is 1.2 mJ of pump energy, corresponding to 50 MW/cm2 average pump intensity which is in agreement with the Brosnan and Byer theory [20], for the case of a singly resonant OPO with pump reflection. A maximum output energy of 0.47 mJ is achieved when 4.4 mJ of pump energy is applied, thus the idler conversion efficiency is 11% and the quantum conversion efficiency is 31% (see Fig. 4a). Even though in our previous work on OPO [16] a much higher energy was presented from an identical oscillator this approach based on short-cavity design, single OPO has significant drawbacks due to the small number of roundtrips that are realizable in the OPO cavity for the duration of the pump pulse which is ≤1 ns. This requires the length of the resonator to be determined by the length of the PPSLT nonlinear crystal and the transverse beam diameter from the damage threshold of the nonlinear crystals or rear mirror. According to our experience, around 3-micron spectral range, the limited factor is the damage of the rear mirror coating which reflects pump at 1 micron and idler around 3 microns, simultaneously. In addition, the shortest cavity design leads to larger Fresnel numbers and the radiation field modes arise which cause a decline in beam quality. However, in the current setup, the output energy and efficiency of the whole system are essentially determined by the OPA, so the OPO can be operated with low-energy pump which is also beneficial for the output beam quality.

Using a knife edge technique [21], the beam diameter of the idler was measured at various positions near the waist using CaF_2 focusing lens with focal length of 50 mm. The estimated beam quality of $M^2 = 31 \times 32$ is shown on Fig. 4b. To measure the idler pulse duration, we frequency doubled the idler pulse using birefringent phase-matched SHG in a 4-mm thick KTP crystal and measured the pulse duration of the generated second harmonic signal (SH) which was 450 and 330 ps for the OPA and OPO output, respectively. The pulse duration measurements have been done

using a InGaAs photodiode connected to a 4 GHz digital oscilloscope. The response time of the measurement system is 160 ps and it was measured with a signal-to-noise-ratio better than 100, and the statistical errors and noise contributions are not substantial (e.g., the RMS of the FWHM of the record response functions is not greater than ~5 ps). After deconvolution, the pulse duration (FWHM) of the frequency-doubled idler is found to be 288 and 420 ps for OPO and OPA, respectively, which corresponds to ~400 and ~600 ps idler duration. The accuracy of the measurement is estimated to be ±25 ps.

The idler output from the OPO is imaged in the OPA with two CaF_2 lenses with focal lengths of 100 and 200 mm resulting in a beam diameter of 3 mm which is slightly larger than the pump beam diameter of 2.8 mm. The maximum of the OPA-seeded idler energy is measured to be ~0.39 mJ at 3.1 µm idler wavelength. It is a reduced OPO output by the Fresnel reflection of the both CaF2-uncoated lenses and transmittance from the dichroic mirror (DM on Fig. 1). When the OPA is pumped with the maximum energy of 29 mJ, the idler energy reaches 4.1 mJ, which corresponds to idler conversion efficiency of 13% and quantum conversion efficiency of 51% (Fig. 5). The setup was operated continuously for several months and no damage in any of the optical elements was observed which renders the system as a reliable source for high-energy mid-IR pulses.

Pulse durations of the incident pump and the second harmonic of the idler pulse from the OPO and OPA are shown in Fig. 6. The estimated pulse duration of the idler pulses after parametric amplification is 600 ps, which indicates the onset of parametric fluorescence; however, the spectral broadening in OPA stage is not substantial (see Fig. 7a). The Idler spectrum is measured with a monochromator and a PbSe detector and the signal spectrum is measured with a commercial NIR spectrometer (Photon Control SPM-002). At 3.1 µm idler canter wavelength and maximum energy output from
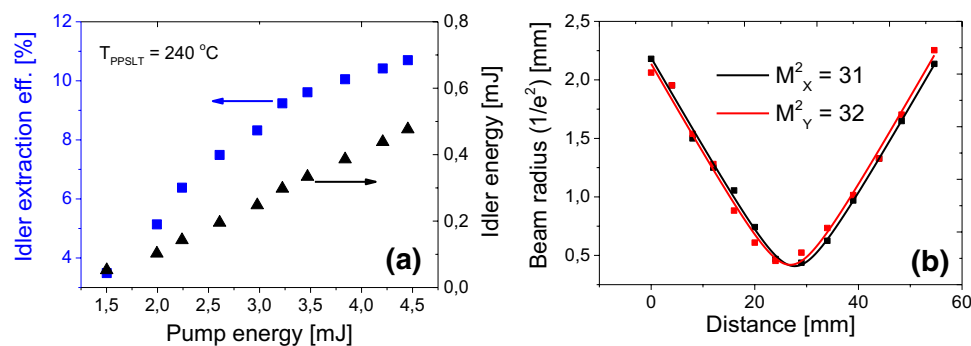

Fig. 4 **a** Idler energy versus pump energy incident on the PPSLT crystal in the OPO at crystal temperature 240 °C (black triangles). The output idler energy is corrected with the transmission of the optical elements. Idler conversion efficiency (blue rectangles); **b** beam

waist along the propagation axis for various positions behind an inserted lens (50 mm). The idler beam quality factor M^2 is measured at 3.1 µm wavelength and pump intensity ≈ 190 MW/cm^2
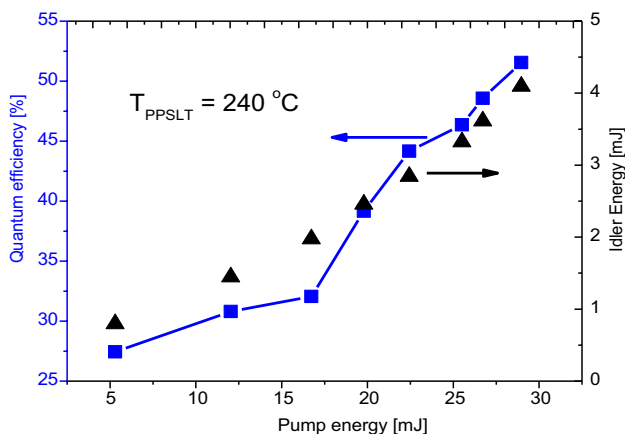
Fig. 5 Idler energy versus pump energy incident on the PPSLT crystal in the OPA at crystal temperature 240 °C (black triangles).The output idler energy is corrected with the transmission of the optical elements. Quantum efficiency (blue rectangles; the blue curve is just for eye guidance)
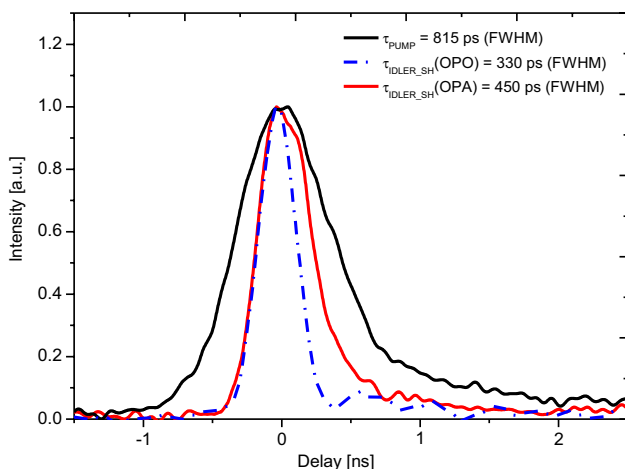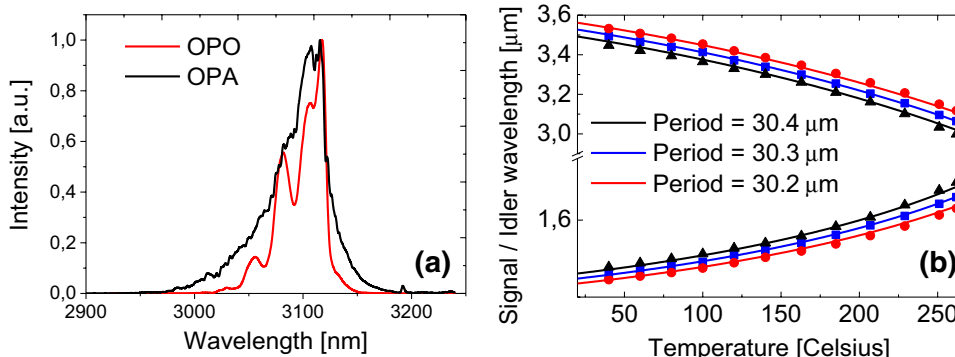

Fig. 6 Temporal pulse shapes of the incident pump and the second harmonic of the idler pulse from the OPO and OPA. Maximum intensity of all pulses is given at the zero time position

the OPA, the idler spectral width is ~ 45 nm (FWHM). The bandwidth of the idler spectrum is determined mostly by the spectral bandwidth of the phase matching for collinear interaction as well as by the divergence of the parametric emission which enables noncollinear phase matching, generating spectral components different from those of collinear phase matching [22]. Parametric gain bandwidth can be evaluated simply in the case of plane-wave collinear interaction [23] for large gain, i.e., for parametric gain coefficient Γ, $\Gamma \gg 1/L$ and $\Gamma \gg \Delta k/2$ gain-half-maximum is approximately given by $\Delta k_{1/2}$:

$$\Delta k_{1/2} = 2\sqrt{(\Gamma \ln 2)/L}$$

$$\Delta k = \left| k_p - k_s - k_i \right|, \quad \Gamma = \left(\frac{2\omega_s \omega_i d_{eff}}{n_i n_s n_p c^3 e_0} I_p \right)^{1/2}$$

L is the nonlinear crystal length, n_i, n_s and n_p are the refractive indices for idler, signal and the pump waves, respectively; k_p, k_s and k_i are the pump, signal and idler wave vectors, respectively, L is the nonlinear crystal length, I_p is the input pump intensity.

In the presented frequency conversion setup, the input pump intensity used for the OPA is higher than the threshold for parametric fluorescence (single-pass optical parametric generation) and much higher than the one used for OPO pumping. The higher pump intensity determines the broader idler OPA spectrum (at least ~ 1.4 times) compared to the OPO spectrum despite its longer crystal length.

By changing the temperature of the PPSLT crystal from room temperature up to 265 °C, we are able to achieve continuous tuning from 3.5 to 3 μm employing the three domain inversion periods (Fig. 7b). The experimental results of OPA wavelengths(solid curves) are in very good agreement with the theoretically calculated curves (solid lines) for the domain inversion periods (Fig. 7b). In the above calculations, we used the Sellmayer coefficients and the expression for thermal expansion of SLT derived by Dolev et al. [24].

Fig. 7 a Idler spectrum measured at maximum output from the OPO (red curve) and after parametric amplification (black curve); **b** OPO temperature tuning for three domain inversion periods, measured data (dots) and calculated tuning curves (solid curves)

In the used temperature range, the chosen PPSLT design provides the wavelength being detuned along the right slope of the water absorption curve at 3 microns, whereby the absorption coefficient changes with few orders of magnitude.

4 Summary and conclusion

We present table-top 1-μm-master oscillator power amplifier system with further frequency conversion to mid-IR. The mid-IR picosecond output (~ 600 ps) is characterized with high energy − 4.1 mJ at 0.5 kHz which results in a high-average power as well. The generated wavelength is tuned near the water absorption peak at 3 μm which is of fundamental interest for medical applications and specifically for minimally invasive surgery. Although the two-stage frequency conversion is more complex than a single OPO, the utilized approach offers more reliability and further scaling of the energy and average power. The obtained results show that the presented laser system is a viable alternative of the mid-IR FELs for potential medical and material science applications as a table-top mid-IR laser.

References

1. G.S. Edwards, R.H. Austin, F.E. Carroll, M.L. Copeland, M.E. Couprie, W.E. Gabella, R.F. Haglund, B.A. Hooper, M.S. Hutson, E.D. Jansen, K.M. Joos, D.P. Kiehart, I. Lindau, J. Miao, H.S. Pratisto, J.H. Shen, Y. Tokutake, van der A.F.G. Meer, A. Xie, Rev. Sci. Instrum. **74**, 3207 (2003). https://doi.org/10.1063/1.1584078
2. A. Vogel, V. Venugopalan, Chem. Rev. **103**, 577 (2003). https://doi.org/10.1021/cr010379n
3. J.I. Youn, P. Sweet, G.M. Peavy, V. Venugopalan, Lasers Surg. Med. **38**, 218 (2006). https://doi.org/10.1002/lsm.20288
4. S. Amini-Nik, D. Kraemer, M.L. Cowan, K. Gunaratne, P. Nadesan, B.A. Alman, R.J.D. Miller, PLoS One **5**(9), e13053 (2010). https://doi.org/10.1371/journal.pone.0013053
5. A. Nierlich, D. Chuchumishev, E. Nagel, K. Marinova, S. Philipov, T. Fiebig, I. Buchvarov, C.P. Richter, Proc. SPIE 8926, Photonic Therapeutics and Diagnostics X, 89262H (2014). https://doi.org/10.1117/12.2049339
6. G.S. Edwards, M.S. Hutson, S. Hauger, Heat Diffusion and Chemical Kinetics in Mark-III FEL Tissue Ablation. Proc. SPIE 4633, pp. 184–193 (2002). https://doi.org/10.1117/12.461378
7. J.T. Walsh, T.F. Deutsch, IEEE Trans. Biomed. Eng. **36**, 1195 (1989). https://doi.org/10.1109/10.42114
8. M.L. Wolbarsht, IEEE J. Quantum Electron. **20**, 1427 (1984). https://doi.org/10.1109/JQE.1984.1072328
9. A. Böttcher, S. Kucher, R. Knecht, N. Jowett, P. Krötz, R. Reimer, U. Schumacher, S. Anders, A. Münscher, C.V. Dalchow, R.J.D. Miller, Eur. Arch. Otorhinolaryngol. **272**, 941 (2015). https://doi.org/10.1007/s00405-015-3501-4
10. G. Edwards, R. Logan, M. Copeland, L. Reinisch, J. Davidson, B. Johnson, R. Maciunas, M. Mendenhall, R. Ossoff, J. Tribble, J. Werkhaven, D. Oday, Nature **371**, 416 (1994). https://doi.org/10.1038/371416a0
11. I.T. Sorokina, K.L. Vodopyanov (eds). *Solid-State Mid-Infrared Laser Sources* (Springer, Berlin Heidelberg, 2003), ISBN 978-3-540-36491-7
12. N. Dixit, R. Mahendra, O.P. Naraniya, A.N. Kaul, A.K. Gupta, Opt. Laser Technol. **42**, 18 (2010). https://doi.org/10.1016/j.optlastec.2009.04.012
13. J. Saikawa, M. Miyazaki, M. Fujii, H. Ishizuki, T. Taira, Opt. Lett. **33**, 1699 (2008). https://doi.org/10.1364/OL.33.001699
14. H. Ishizuki, T. Taira, Opt. Express **18**, 253 (2010). https://doi.org/10.1364/OE.18.000253
15. M. Katz, P. Blau, B. Shulga: Proc. SPIE 6875, p. 687504-14 (2008). https://doi.org/10.1117/12.763190
16. D. Chuchumishev, A. Gaydardzhiev, T. Fiebig, I. Buchvarov, Opt. Lett. **38**, 3347 (2013). https://doi.org/10.1364/OL.38.003347
17. V. Evtuhov, A.E. Siegman, Appl. Opt. **4**, 142 (1965). https://doi.org/10.1364/AO.4.000142
18. M. Ostermeyer, G. Klemz, P. Kubina, R. Menzel, Appl. Opt. **41**, 7573 (2002). https://doi.org/10.1364/AO.41.007573
19. B. Oreshkov, D. Chuchumishev, H. Iliev, A. Trifonov, T. Fiebig, C.P. Richter, I. Buchvarov, *CLEO 2014, OSA Technical Digest (online)* (Optical Society of America, 2014), paper JW2A.84. https://doi.org/10.1364/CLEO_AT.2014.JW2A.84
20. S. Brosnan, R.L. Byer, IEEE J. Quantum Electron. **15**, 415 (1979). https://doi.org/10.1109/JQE.1979.1070027
21. A. Siegman, M. Dowley, Proc. Optical Society of America 17, p. MQ1 (1998). https://doi.org/10.1364/DLAI.1998.MQ1
22. A. Seilmeier, K. Spanner, A. Laubereau, W. Kaiser, Opt. Commun. (1978). https://doi.org/10.1016/0030-4018(78)90001-9
23. R.A. Baumgartner, R.L. Byer, IEEE J. Quantum Electron. **15**, 432 (1979). https://doi.org/10.1109/JQE.1979.1070043
24. I. Dolev, A. Ganany-Padowicz, O. Gayer, A. Arie, J. Mangin, G. Gadret, Appl. Phys. B **96**, 423 (2009). https://doi.org/10.1007/s00340-009-3502-3